Research Square

Preprints are preliminary reports that have not undergone peer review.
They should not be considered conclusive, used to inform clinical practice,
or referenced by the media as validated information.

Synergistic Effect of Mn and V in Regulating Low-Ruthenium Oxide Nanowires for Highly Efficient and Stable Acidic Water Oxidation

Jianyun Liu

2754580538@qq.com

Shanghai Branch, Envision Energy Co., Ltd.

Research Article

Keywords: acidic water oxidation, ruthenium-based oxides, manganese-vanadium modulation, synergistic effect, proton exchange membrane water electrolysis

Posted Date: November 12th, 2026

DOI: https://doi.org/10.21203/rs.3.rs-11501698/v1

License: This work is licensed under a Creative Commons Attribution 4.0 International License.
Read Full License

Additional Declarations: No competing interests reported.

Synergistic Effect of Mn and V in Regulating Low-Ruthenium Oxide Nanowires for Highly Efficient and Stable Acidic Water Oxidation

Jianyun Liu†

†Shanghai Branch, Envision Energy Co., Ltd., Shanghai 200023, China.

E-mail: 2754580538@qq.com

Abstract

Suppressing the dissolution of Ru sites in Ru-based oxides during the oxygen evolution reaction (OER) in acidic media is a critical challenge for the development of low-cost proton exchange membrane water electrolysis (PEMWE) technology. In this study, $Ru_{0.2}V_{0.05}Mn_{0.75}O_2$ nanowires were synthesized via a hydrothermal method. Through the synergistic effect of Mn and V, the crystal structure and the bond energy of the Ru–O bonds in the Ru-based oxide were effectively modulated. The $Ru_{0.2}V_{0.05}Mn_{0.75}O_2$ catalyst exhibited OER overpotentials of 212 and 295 mV at 10 and 50 mA cm^{-2} respectively in 0.5 M H_2SO_4, values 132 and 148 mV lower than those of pure RuO_2. When employed as an anode in a PEMWE cell, $Ru_{0.2}V_{0.05}Mn_{0.75}O_2$ achieved a cell voltage of only 1.61 V at a current density of 1 A cm^{-2} and demonstrated stable operation for over 250 hours. Electrochemical impedance spectroscopy (EIS) analysis revealed that the incorporation of Mn and V helps reduce charge-transfer resistance during the OER. Furthermore, inductively coupled plasma optical emission spectroscopy (ICP-OES) and density functional theory (DFT) calculations indicate that the synergistic effect of Mn and V increases the vacancy formation energy of Ru sites—from 1.68 eV in RuO_2 to 2.75 eV in $Ru_{0.2}V_{0.05}Mn_{0.75}O_2$—thereby effectively suppressing the dissolution of Ru sites during the OER process and enhancing the structural stability of the material.

Keywords: acidic water oxidation; ruthenium-based oxides; manganese-vanadium modulation; synergistic effect; proton exchange membrane water electrolysis

Introduction

Hydrogen production via water electrolysis powered by renewable electricity is a crucial pathway for low-carbon energy conversion and storage [1]. Proton exchange membrane water electrolysis (PEMWE) offers advantages such as high current density, high gas purity, and excellent dynamic response [2, 3]. However, the oxygen evolution reaction (OER) at the anode involves a complex four-electron transfer process and occurs in a highly acidic, high-oxidative-potential environment, placing stringent demands on the activity and structural stability of the catalysts [4-6]. Iridium-based catalysts are currently the primary materials used for PEMWE anodes; however, the scarcity and high cost of iridium limit their large-scale application. In contrast, RuO_2 is considered a promising next-generation anode catalyst to replace iridium-based materials because of its high OER activity in acidic media and lower costs [7-9]. Nevertheless, the highly acidic and oxidative environment at the anode can lead to the over-oxidation of Ru sites, forming unstable high-valence species that trigger Ru dissolution and cause a gradual increase in the cell voltage of the PEMWE system [10-12]. Consequently, suppressing Ru dissolution while maintaining high-efficiency oxygen evolution is the key to developing long-term stable ruthenium-based catalysts for acidic OER [13-15].

The stability of ruthenium-based oxides is closely linked to Ru–O bonding and local electronic structure [16-18]. Ru^{4+} possesses a $4d^4$ electronic configuration, where the hybridization between its 4d orbitals and the O 2p orbitals influences the redox behavior of the metal and the binding of oxygen-containing species [19, 20]. At high potentials, both the over-oxidation of Ru and the loss of local oxygen coordination can facilitate the dissolution of Ru sites [21, 22]. Modulating the electron distribution and coordination environment of Ru sites has emerged as an effective strategy to enhance the stability of ruthenium-based oxides for acidic water oxidation [23-26]. For instance, Wu et al. developed a Ni-stabilized Ni–RuO_2 system, which improves durability by stabilizing Ru atoms in the surface layer and O atoms in the subsurface layer [7]. Similarly, Hu et al. employed a one-step synthesis method to produce $RuTiO_x$, which features a Ru–O–Ti

structure that prevents catalyst deactivation caused by the over-oxidation of Ru during the OER process [27]. These studies indicate that the dissolution of Ru atoms can be effectively suppressed by modulating the Ru–O bond energy and the local electronic structure of Ru [28-30]. Mn and V can adopt multiple oxidation states and may influence the local coordination and electronic environment of Ru sites [31, 32]. Wang et al. discovered that the redistribution of electrons between Ru and Mn—mediated by bridging oxygen—improves the adsorption and conversion of oxygen-containing intermediates [33]. Meanwhile, Liu et al. found that in V-modified RuO_2, V can modulate the Lewis acidity of the Ru sites to facilitate the deprotonation of water molecules, while also acting as a redox buffer to mitigate the over-oxidation of Ru [34]. Therefore, by optimizing the local electronic structure and deprotonation capability of Ru through the synergistic effect of manganese and vanadium, it is possible to simultaneously enhance both the stability and activity of ruthenium-based oxide catalysts.

Herein, we developed a flexible hydrothermal method to synthesize the Ru–V–Mn multimetallic oxide. The optimized $Ru_{0.2}V_{0.05}Mn_{0.75}O_2$ displays low overpotentials of 212 and 295 mV at 10 and 50 mA cm^{-2} for OER in 0.5 M H_2SO_4, respectively. It can also work at a low voltage of 1.61 V with a stable response at a current density of 1 A cm^{-2} when being coupled with Pt/C in a PEMWE. Inductively coupled plasma optical emission spectroscopy (ICP-OES) and density functional theory (DFT) calculations further reveal that the incorporation of Mn and V effectively increases the vacancy formation energy of Ru, significantly inhibiting the dissolution of active Ru sites during the OER, which confirms that multi-metal modulation enhances the structural stability of Ru sites. Additionally, the combined incorporation of Mn and V reduces the interfacial resistance during the OER process, thereby boosting the catalytic activity of the $Ru_{0.2}V_{0.05}Mn_{0.75}O_2$ material.

Experimental Section

Synthesis Methods

Fabrication of RuO_2 powder: 0.2 mmol of $RuCl_3 \cdot xH_2O$ (99%, Innochem) and 8 mL of 2 mol L^{-1} NaOH (95%, Aladdin) solution were added to 30 mL of deionized water and stirred

for 10 min. The resulting mixture was then transferred into a 100 mL Teflon-lined autoclave and heated at 150 °C for 10 h. After the reaction, the generated precipitate was centrifuged and separated with a mixture of ethanol and deionized water several times. The precipitate was freeze-dried and ground, and the resulting powder was calcined in air at 600 °C for 6 h to obtain RuO_2 powder.

Fabrication of $Ru_{0.2}Mn_{0.8}O_2$ nanowire catalyst: 2.56 mmol of $KMnO_4$ (99%, Innochem), 0.96 mmol of $MnSO_4·H_2O$ (99%, Aladdin), and 0.88 mmol of $RuCl_3·xH_2O$ (99%, Innochem) were added to 32 mL of deionized water and stirred for 30 min. The mixture was then transferred into a 100 mL Teflon-lined autoclave and heated at 160 °C for 12 h. After the reaction, the generated precipitate was centrifuged and separated with a mixture of ethanol and deionized water several times. Finally, the precursor was heat-treated in air at 250 °C for 2 h to obtain $Ru_{0.2}Mn_{0.8}O_2$ powder.

Fabrication of Ru–V–Mn multimetallic oxide nanowire catalyst: 1.92 mmol of $KMnO_4$ (99%, Innochem), 0.72 mmol of $MnSO_4·H_2O$ (99%, Aladdin), 0.88 mmol of $RuCl_3·xH_2O$ (99%, Innochem), and 0.22 mmol of $VOSO_4$ (99%, Innochem) were added to 32 mL of deionized water. After stirring for 30 min, the mixture was transferred into a 100 mL Teflon-lined autoclave and heated at 160 °C for 12 h. After the reaction, the generated precipitate was centrifuged and separated with a mixture of ethanol and deionized water several times. It was then subjected to heat treatment in an air atmosphere at 250 °C for 2 h to obtain $Ru_{0.2}V_{0.05}Mn_{0.75}O_2$ powder. To investigate the effect of V content on material properties, the amounts of $VOSO_4$, $KMnO_4$, and $MnSO_4·H_2O$ were adjusted while keeping the quantity of $RuCl_3·xH_2O$ constant (0.88 mmol). The resulting samples were labeled as $Ru_{0.2}V_{0.01}Mn_{0.79}O_2$、$Ru_{0.2}V_{0.08}Mn_{0.72}O_2$ and $Ru_{0.2}V_{0.1}Mn_{0.7}O_2$, respectively.

Fabrication of Ru–V–MnO_x-loaded electrodes: A mixture of 5 mg of the catalyst and 5 mg of Vulcan XC-72 carbon powder was dispersed in 1 mL of a solvent mixture consisting of deionized water and isopropanol (99%, Aladdin) in a 3:1 volume ratio. Then, 40 μL of a 5 wt% Nafion solution was added as a binder. After 30 min of ultrasonic dispersion, 30 μL of homogeneous ink was dropped on a carbon paper substrate (Fuel Cell Earth, TGP-H-060) (area, 0.25 cm^2) and fully dried in air at room temperature. The mass loadings of the electrocatalysts onto carbon paper were controlled at approximately 0.6 mg cm^{-2}.

Fabrication of Pt/C-Loaded Electrodes: A commercial 20% Pt/C catalyst was dispersed in 1 mL of isopropanol (99%, Aladdin). Then, 40 μL of a 5 wt% Nafion solution was added, and the mixture was ultrasonically dispersed for 30 min to obtain a uniform catalyst ink. Subsequently, the ink was applied onto a carbon paper substrate (Fuel Cell Earth, TGP-H-060) with an area of 0.25 cm^2, with the mass loading of the Pt/C catalyst controlled at 0.6 mg cm^{-2}.

Material characterizations

The microscopic morphology of the materials was observed using a Tecnai G2 transmission electron microscope (FEI, USA). The crystal structure was analyzed via X-ray diffraction (XRD) using a DMAX-2400 diffractometer (Rigaku, Japan). The elemental composition was determined using an EAGLE III X-ray fluorescence (XRF) spectrometer at an operating voltage of 40 kV. ICP-OES was employed for the quantitative analysis of metal elements.

Electrochemical characterization

The OER polarization curves were carried out with a CHI 760D (Chenhua, China) electrochemical workstation in 0.5 M H_2SO_4 electrolyte in a typical three-electrode system with a scan rate of 5 mV s^{-1} at room temperature. A standard three-electrode system was utilized, consisting of the catalyst-loaded electrode as the working electrode, an Ag/AgCl electrode as the reference electrode, and a commercial carbon rod as the counter electrode. All measured potentials were calibrated against the reversible hydrogen electrode (RHE) scale by determining the potential difference between the Ag/AgCl reference electrode and the RHE.

Proton exchange membrane (PEM) electrolyzer

A membrane electrode assembly (MEA) was fabricated using a Nafion®117 polymer membrane (DuPont, thickness 177.8 μm, N117). Prior to assembly, the N117 membrane was subjected to a series of boiling treatments—each lasting 30 minutes—in 3 wt% H_2O_2 solution, Milli-Q ultrapure water, 1.0 mol L^{-1} H_2SO_4 solution, and finally Milli-Q ultrapure water again. This process removes potential contaminants and ensures the membrane is

fully protonated. The treated membrane was then dried in an oven at 40 °C for several hours before use.

$Ru_{0.2}V_{0.05}Mn_{0.75}O_2$ and commercial Pt/C were employed as the anode and cathode catalysts, respectively, with mass loadings controlled at 1 mg cm^{-2} and 0.2 mg cm^{-2}. The effective area of the MEA was 5 cm^2. Electrolysis tests were carried out in a single-cell PEM water electrolyzer, utilizing titanium mesh as the gas diffusion layer for both the anode and the cathode. During the test, the electrolytic cell was maintained at room temperature, and preheated deionized water was delivered to the anode at a flow rate of 10 mL min^{-1} through tubing with a diameter of 4.8 mm.

Computational Details

The DFT calculations were carried out via the Vienna ab initio simulation package (VASP) [35, 36]. The ion-electron interaction was described with the projector augmented-wave (PAW) method [37]. The exchange-correlation energy was treated using the Perdew-Burke-Ernzerhof (PBE) functional within the generalized gradient approximation (GGA) [38].

The formation energy of a Ru vacancy was calculated according to the following equation:

$$E_f = E_{vac} - E_{pure} + E_{Ru}$$

where E_{vac} and E_{pure} are the total energies of the system with and without Ru vacancy, respectively. E_{Ru} is the energy per atom of bulk Ru.

Results and Discussion

Synthesis and structural characterization

Ru–V–Mn multimetallic oxides were synthesized by a hydrothermal method and then annealed in air at 250 °C for 2 hours. $Ru_{0.2}Mn_{0.8}O_2$ was prepared using the same hydrothermal and heat-treatment processes; meanwhile, RuO_2 was used as a reference to compare the effects of incorporating Mn and V on the material's structure and oxygen evolution performance.



Fig.1 Schematic synthetic procedure for Ru–V–Mn multimetallic oxide nanowires.

First, XRF spectroscopy was employed to analyze the metallic elemental composition of the samples (Fig. 2a). The atomic ratio of Ru:Mn in $Ru_{0.2}Mn_{0.8}O_2$ is 20.15%: 79.85%, while the atomic ratio of Ru: V: Mn in $Ru_{0.2}V_{0.05}Mn_{0.75}O_2$ is 20.34%: 5.65%: 74.01%. Both values are close to the target stoichiometric ratios, indicating that the Ru cation proportions in the two multimetallic oxides are similar, and that the introduction of V primarily corresponds to the partial substitution of Mn. Fig. 2b presents the XRD patterns of the three materials. The diffraction peaks of RuO_2 correspond to the (110), (101), and (211) planes of RuO_2 (PDF# 43-1027). Upon the incorporation of Mn and V, the samples retain similar XRD diffraction peaks, indicating that they possess the primary structural characteristics of rutile-type oxides. Compared to RuO_2 and $Ru_{0.2}Mn_{0.8}O_2$ the diffraction peaks of $Ru_{0.2}V_{0.05}Mn_{0.75}O_2$ exhibit significant broadening which suggests that the introduction of V alters the crystalline state of the material, likely due to an increase in local structural disorder within $Ru_{0.2}V_{0.05}Mn_{0.75}O_2$ [39, 40]. In conjunction with the XRF results, it is evident that while the incorporation of multiple metallic components preserves the primary crystal structure, it also affects the structural order of the material. Furthermore, the XRD pattern of these Ru–V–Mn multimetallic oxide catalysts with different Mn: V ratios shows the same phase structure, and their XRD diffraction peaks can be referred to RuO_2 (PDF# 43-1027) (Fig. S1, Supporting Information).

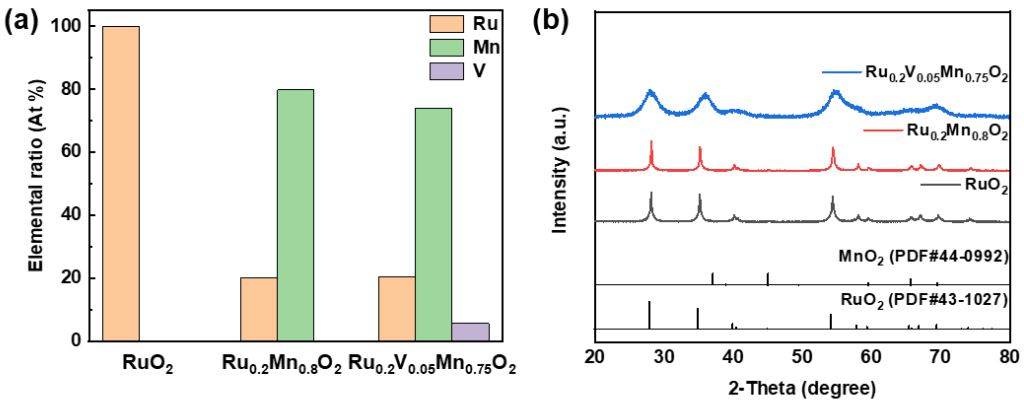


Fig. 2 (a) XRF and (b) XRD patterns of RuO_2, $Ru_{0.2}Mn_{0.8}O_2$ and $Ru_{0.2}V_{0.05}Mn_{0.75}O_2$.

TEM was employed to further characterize the microscopic morphology of the materials. RuO_2 appears as small particles with a diameter of approximately 30 nm, exhibiting significant aggregation (Fig. 3a). In contrast, $Ru_{0.2}Mn_{0.8}O_2$ displays a smooth nanowire morphology, with some particles attached to the surface (Fig. 3b). Upon co-doping with Mn and V, the $Ru_{0.2}V_{0.05}Mn_{0.75}O_2$ catalyst exhibits a rough nanowire structure (Fig. 3c). RuO_2 consists of aggregated particles, whereas the Mn and V containing samples exhibit nanowire morphologies under their respective synthesis conditions. Such a rough nanowire structure may help expose more reaction sites, thereby enhancing the catalytic activity of the material [41, 42]. Elemental mapping of $Ru_{0.2}V_{0.05}Mn_{0.75}O_2$ reveals that Mn, O, Ru, and V are uniformly distributed throughout the nanowires (Fig. 3d).

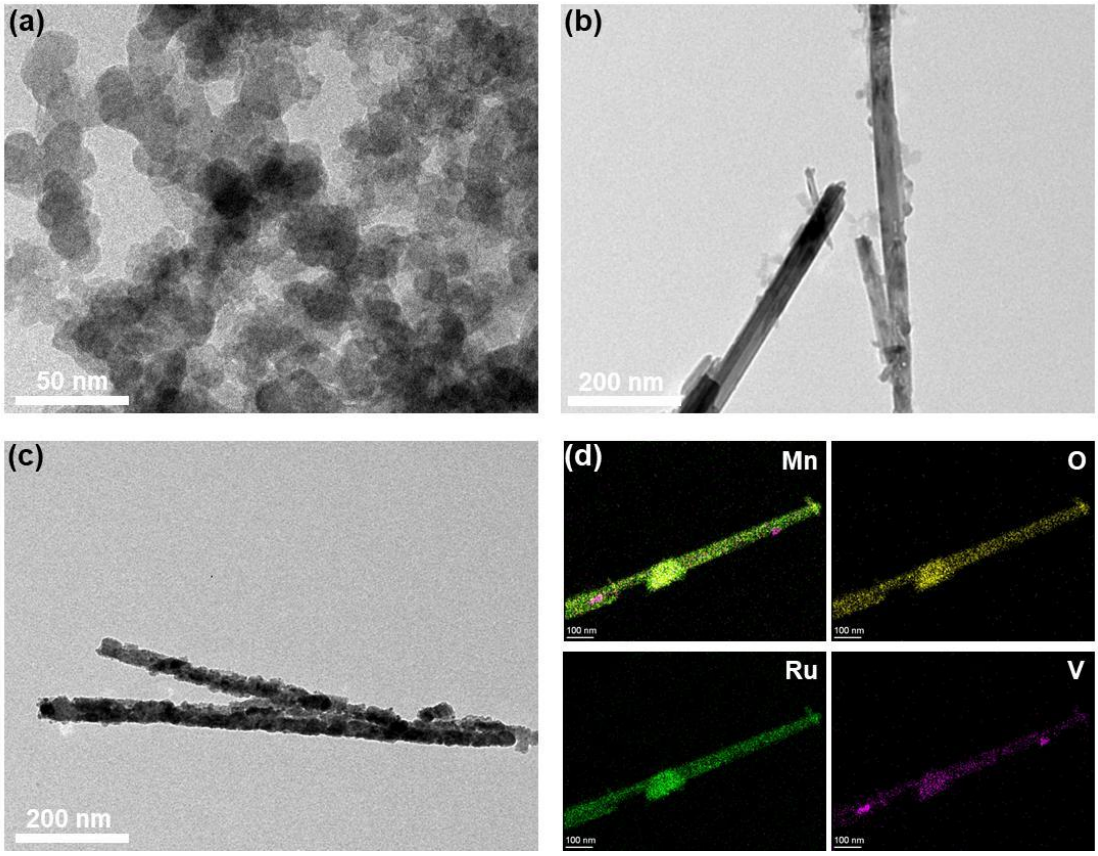


Fig. 3 (a-c) TEM images of RuO_2, $Ru_{0.2}Mn_{0.8}O_2$ and $Ru_{0.2}V_{0.05}Mn_{0.75}O_2$. (d) The corresponding elemental mappings of Mn, O, Ru and V of $Ru_{0.2}V_{0.05}Mn_{0.75}O_2$.

Catalytic performance of Ru–V–Mn multimetallic oxides for OER

The OER activity of the materials was evaluated in a 0.5 mol L^{-1} H_2SO_4 solution at room temperature. As shown in Fig. 4a, both $Ru_{0.2}Mn_{0.8}O_2$ and $Ru_{0.2}V_{0.05}Mn_{0.75}O_2$ exhibit superior OER catalytic performance compared to pure RuO_2 particles. At the current density of 10 mA cm^{-2}, the overpotentials for RuO_2, $Ru_{0.2}Mn_{0.8}O_2$, and $Ru_{0.2}V_{0.05}Mn_{0.75}O_2$ are 344, 269, and 212 mV, respectively, and at the current density of 50 mA cm^{-2}, the corresponding overpotentials are 443, 358, and 295 mV. The $Ru_{0.2}V_{0.05}Mn_{0.75}O_2$ catalyst shows a reduction in overpotential of 132 mV and 148 mV, respectively, compared to RuO_2, demonstrating the highest OER catalytic activity. Notably, despite having a similar Ru content to $Ru_{0.2}Mn_{0.8}O_2$, the $Ru_{0.2}V_{0.05}Mn_{0.75}O_2$ sample exhibits an even lower OER overpotential, indicating that the partial substitution of Mn with V further enhances the

OER performance. The Tafel plots are presented in Fig. 4b. Both $Ru_{0.2}Mn_{0.8}O_2$ and $Ru_{0.2}V_{0.05}Mn_{0.75}O_2$ exhibit lower Tafel slopes than RuO_2, suggesting that the incorporation of Mn and V effectively optimizes the electronic structure of the Ru-O active sites, which can optimize the OER energy barrier for $Ru_{0.2}V_{0.05}Mn_{0.75}O_2$. Furthermore, compared to $Ru_{0.2}V_{0.01}Mn_{0.79}O_2$, $Ru_{0.2}V_{0.08}Mn_{0.72}O_2$ and $Ru_{0.2}V_{0.1}Mn_{0.7}O_2$, the $Ru_{0.2}V_{0.05}Mn_{0.75}O_2$ material exhibits the lowest OER overpotential (Fig. S2, Supporting Information).

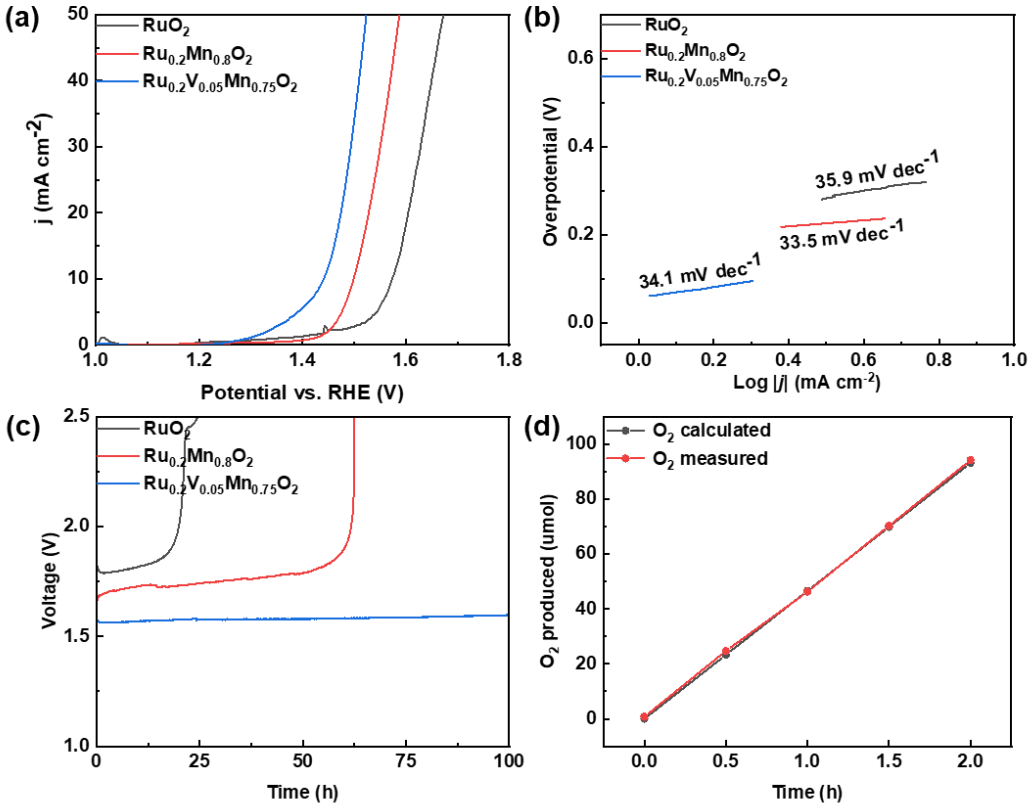


Fig. 4 Electrochemical performance of the studied catalysts in 0.5 M H_2SO_4. (a) OER activity and (b) the corresponding Tafel plots of RuO_2, $Ru_{0.2}Mn_{0.8}O_2$ and $Ru_{0.2}V_{0.05}Mn_{0.75}O_2$. (c) Durability tests of RuO_2, $Ru_{0.2}Mn_{0.8}O_2$ and $Ru_{0.2}V_{0.05}Mn_{0.75}O_2$ electrodes under a constant current density of 50 mA cm^{-2} for 100 h. (d) The amount of generated oxygen (by theoretical calculation and experimental measurement) versus time for $Ru_{0.2}V_{0.05}Mn_{0.75}O_2$ at a current density of 10 mA cm^{-2}.

The stability of RuO_2, $Ru_{0.2}Mn_{0.8}O_2$, and $Ru_{0.2}V_{0.05}Mn_{0.75}O_2$ electrodes was compared via chronopotentiometric testing at a current density of 50 mA cm^{-2} (Fig. 4c). The voltage for

RuO_2 rises rapidly within 25 h, whereas the $Ru_{0.2}Mn_{0.8}O_2$ electrode maintains stable operation for 60 h. For the $Ru_{0.2}V_{0.05}Mn_{0.75}O_2$ catalyst, no significant voltage increase is observed over 100 h. Stability test results indicate that the combined incorporation of Mn and V effectively suppresses the performance degradation of Ru-based oxide catalysts, thereby extending their operational lifespan. Furthermore, the Faradaic efficiency of $Ru_{0.2}V_{0.05}Mn_{0.75}O_2$ is close to 100%, indicating that the current is primarily consumed by the OER under the tested conditions (Fig. 4d).

In addition, we assembled a PEMWE (Fig. 5a). $Ru_{0.2}V_{0.05}Mn_{0.75}O_2$ materials and the commercial Pt/C catalysts were used as the anode and cathode in PEMWE, respectively. As shown in Fig. 5b, the PEM electrolyzer utilizing the optimized $Ru_{0.2}V_{0.05}Mn_{0.75}O_2$ electrocatalyst exhibited a cell voltage of 1.61 V at a current density of 1 A cm^{-2} and remained stable for at least 250 hours without any significant performance degradation. These results demonstrate that $Ru_{0.2}V_{0.05}Mn_{0.75}O_2$ can operate continuously at ampere-level current densities, confirming its potential for application as an anode catalyst in commercial acidic water electrolysis.

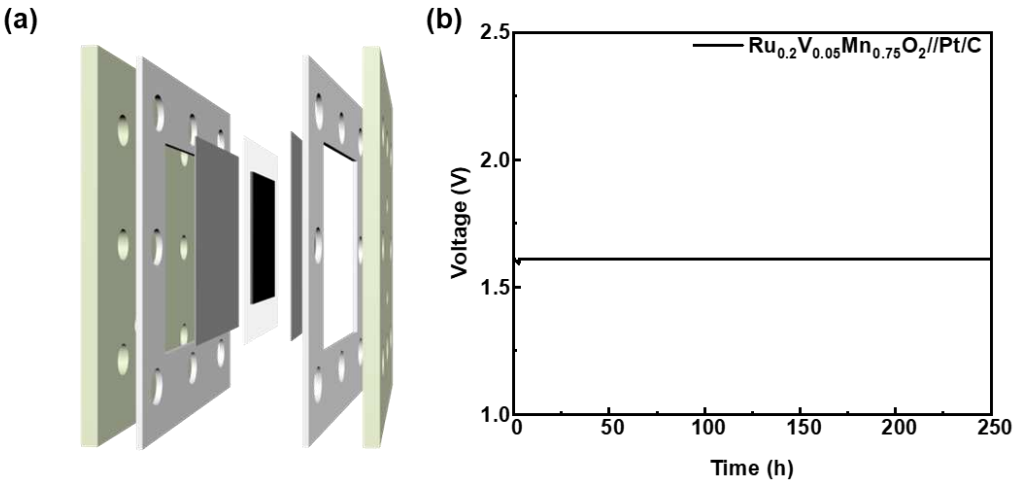


Fig. 5 (a) Schematic diagram of the PEM electrolyser. (b) Chronopotentiometry tests of the $Ru_{0.2}V_{0.05}Mn_{0.75}O_2$ catalyst at 1 A cm^{-2} in the PEMWE.

Mechanism Study

Electrochemical impedance spectroscopy (EIS) measurements of RuO_2, $Ru_{0.2}Mn_{0.8}O_2$, and $Ru_{0.2}V_{0.05}Mn_{0.75}O_2$ electrodes were tested at 1.48 V vs. RHE in 0.5 M H_2SO_4 (Fig. 6a). Among these samples, $Ru_{0.2}V_{0.05}Mn_{0.75}O_2$ exhibits the smallest impedance arc, pointing to the lowest charge transfer resistance and the fastest charge transfer rate for OER. The OER performance of $Ru_{0.2}V_{0.05}Mn_{0.75}O_2$ is also investigated [43]. Consequently, the combined incorporation of Mn and V enhances the OER catalytic activity of Ru-based oxides by increasing the electroactive surface area of the nanowires and reducing charge-transfer resistance.

The XRD patterns of the electrodes after the 30 min stability test (Fig. 6b) show that the RuO_2, $Ru_{0.2}Mn_{0.8}O_2$, and $Ru_{0.2}V_{0.05}Mn_{0.75}O_2$ catalysts all retain the rutile-type RuO_2 phase structure, indicating that no significant phase structural changes occurred in any of these electrodes following the 30 min stability test. ICP-OES was employed to analyze the dissolution of Ru sites in RuO_2, $Ru_{0.2}Mn_{0.8}O_2$, and $Ru_{0.2}V_{0.05}Mn_{0.75}O_2$ catalysts following stability testing (Fig. 6c). Among these materials, the $Ru_{0.2}V_{0.05}Mn_{0.75}O_2$ catalyst exhibited the lowest degree of Ru site dissolution—only 39.3% of that observed for RuO_2. This confirms that the combined incorporation of Mn and V suppresses the dissolution of Ru sites during OER. This further confirms that the synergistic effect of Mn and V can effectively increase the Ru–O bond energy, thereby suppressing the dissolution of Ru ions, which further confirms the long-term stability of $Ru_{0.2}V_{0.05}Mn_{0.75}O_2$.

DFT calculations were employed to further elucidate the reasons for the high stability of $Ru_{0.2}V_{0.05}Mn_{0.75}O_2$. A higher vacancy formation energy for Ru atoms in a catalyst indicates that it is more difficult for these atoms to detach from the material, thereby conferring greater stability. As shown in Fig. 6d, the Ru vacancy formation energies for RuO_2, $Ru_{0.2}Mn_{0.8}O_2$, and $Ru_{0.2}V_{0.05}Mn_{0.75}O_2$ are 1.68 eV, 2.25 eV, and 2.75 eV, respectively, with $Ru_{0.2}V_{0.05}Mn_{0.75}O_2$ exhibiting the highest value. This demonstrates that the Ru–O–Mn bonds, formed through the synergistic interaction between Mn and V, can effectively enhance the bond energy of the Ru–O bonds. Simultaneously, the incorporation of V suppresses the over-oxidation of Ru sites during the OER process [34], thereby improving the stability of the electrocatalyst. This conclusion is also consistent with the results obtained from ICP-OES.

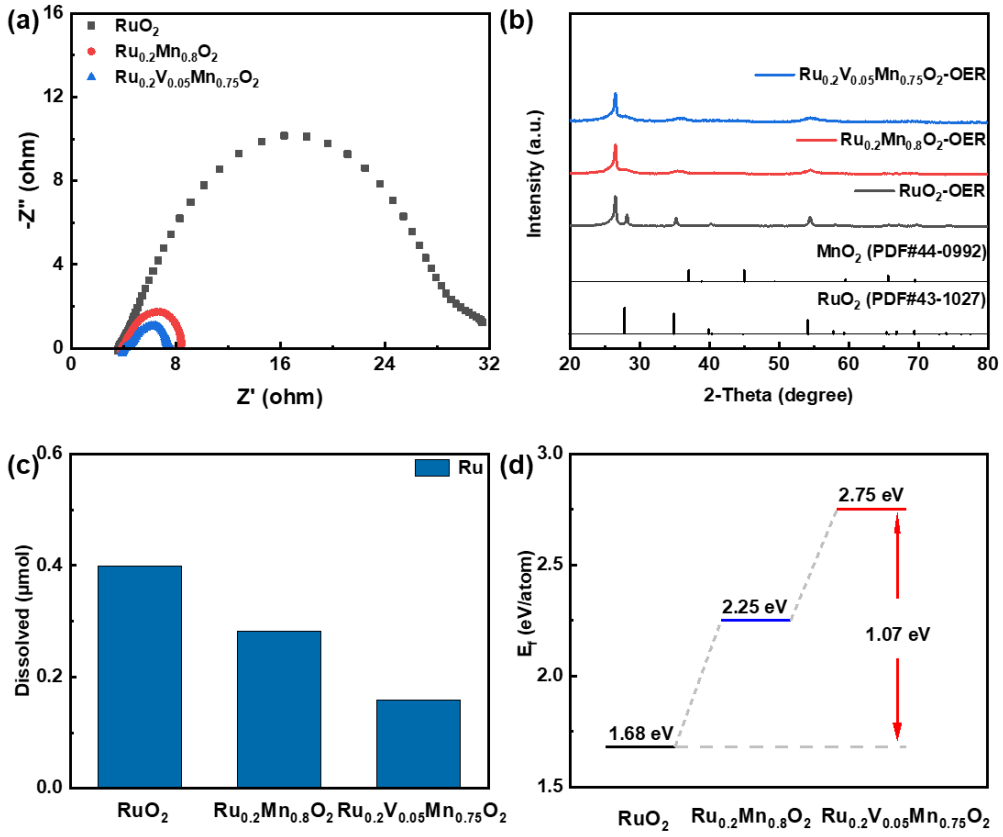


Fig. 6 (a) EIS of RuO_2, $Ru_{0.2}Mn_{0.8}O_2$ and $Ru_{0.2}V_{0.05}Mn_{0.75}O_2$ at the 1.48 V vs. RHE. (b) The XRD patterns of RuO_2, $Ru_{0.2}Mn_{0.8}O_2$ and $Ru_{0.2}V_{0.05}Mn_{0.75}O_2$ after the 30 min stability test. (c) ICP-OES of RuO_2, $Ru_{0.2}Mn_{0.8}O_2$ and $Ru_{0.2}V_{0.05}Mn_{0.75}O_2$. (d) Calculation results of Ru vacancy formation energy for RuO_2, $Ru_{0.2}Mn_{0.8}O_2$ and $Ru_{0.2}V_{0.05}Mn_{0.75}O_2$.

Conclusion

In summary, we have developed a facile hydrothermal method to synthesize $Ru_{0.2}V_{0.05}Mn_{0.75}O_2$ nanowires, which effectively enhance both the OER activity and stability of Ru-based oxides in acidic media. Compared to RuO_2 and $Ru_{0.2}Mn_{0.8}O_2$, $Ru_{0.2}V_{0.05}Mn_{0.75}O_2$ exhibits a rough nanowire morphology, the smallest interfacial charge-transfer resistance, and the lowest oxygen evolution overpotential, which indicates that the synergistic effect of Mn and V can effectively optimize the electrode reaction performance of oxides with low ruthenium content. In 0.5 mol L^{-1} H_2SO_4, this

catalyst exhibits overpotentials of only 212 mV and 295 mV at current densities of 10 mA cm^{-2} and 50 mA cm^{-2}, respectively. When employed as an anode in the PEMWE, it achieves a cell voltage of 1.61 V at a current density of 1 A cm^{-2} and demonstrates stable operation for over 250 hours. DFT calculations further reveal that the synergistic effect of Mn and V increases the formation energy of Ru vacancies, from 1.68 eV to 2.25 eV and 2.75 eV, respectively, thereby effectively suppressing the dissolution of Ru sites during OER. We believe this work may provide guidance for the design of efficient Ru-based oxide electrocatalysts for acidic water oxidation at low overpotential.

Declarations

Acknowledgments

Funding

No funding was received for this study.

Author contributions

J.L. independently carried out the synthesis and the material characterizations, electrochemical experiments, DFT calculation and data analysis.

Competing interests

The authors declare no competing interests.

Data availability

All data generated or analyzed in this study are included in this article and its supplementary information files.

References

1. Chatenet M, Pollet BG, Dekel DR, Dionigi F, Deseure J, Millet P, et al. Water electrolysis: from textbook knowledge to the latest scientific strategies and industrial

developments. Chem Soc Rev. 2022;51(11):4583-762. https://doi.org/10.1039/d0cs01079k
2. Wang CR, Stansberry JM, Mukundan R, Chang HMJ, Kulkarni D, Park AM, et al. Proton exchange membrane (PEM) water electrolysis: cell-level considerations for gigawatt-scale deployment. Chem Rev. 2025;125(3):1257-302. https://doi.org/10.1021/acs.chemrev.3c00904
3. Qiu C, Sellers C, Wu ZY, Cullen DA, Stavitski E, Tayal A, et al. Low-iridium stabilized ruthenium oxide anode catalyst for durable proton-exchange membrane water electrolysis. Nat Nanotechnol. 2025;20(12):1787-95. https://doi.org/10.1038/s41565-025-02030-y
4. An L, Wei C, Lu M, Liu H, Chen Y, Scherer GG, et al. Recent development of oxygen evolution electrocatalysts in acidic environment. Adv Mater. 2021;33(20):2006328. https://doi.org/10.1002/adma.202006328
5. Man IC, Su HY, Calle‐Vallejo F, Hansen HA, Martínez JI, Inoglu NG, et al. Universality in oxygen evolution electrocatalysis on oxide surfaces. ChemCatChem. 2011;3(7):1159-65. https://doi.org/10.1002/cctc.201000397
6. Zheng YR, Vernieres J, Wang Z, Zhang K, Hochfilzer D, Krempl K, et al. Monitoring oxygen production on mass-selected iridium–tantalum oxide electrocatalysts. Nat Energy. 2022;7(1):55-64. https://doi.org/10.1038/s41560-021-00948-w
7. Wu ZY, Chen FY, Li B, Yu SW, Finfrock YZ, Meira DM, et al. Non-iridium-based electrocatalyst for durable acidic oxygen evolution reaction in proton exchange membrane water electrolysis. Nat Mater. 2023;22(1):100-8. https://doi.org/10.1038/s41563-022-01380-5
8. Zhang J, Fu X, Kwon S, Chen K, Liu X, Yang J, et al. Tantalum-stabilized ruthenium oxide electrocatalysts for industrial water electrolysis. Science. 2025;387(6729):48-55. https://doi.org/10.1126/science.ado9938
9. Tang J, Guan D, Xu H, Zhao L, Arshad U, Fang Z, et al. Undoped ruthenium oxide as a stable catalyst for the acidic oxygen evolution reaction. Nat Commun. 2025;16(1):801. https://doi.org/10.1038/s41467-025-56188-z
10. Hao S, Liu M, Pan J, Liu X, Tan X, Xu N, et al. Dopants fixation of ruthenium for boosting acidic oxygen evolution stability and activity. Nat Commun. 2020;11(1):5368. https://doi.org/10.1038/s41467-020-19212-y
11. Xue Y, Zhao J, Huang L, Lu YR, Malek A, Gao G, et al. Stabilizing ruthenium dioxide with cation-anchored sulfate for durable oxygen evolution in proton-exchange membrane water electrolyzers. Nat Commun. 2023;14(1):8093. https://doi.org/10.1038/s41467-023-43977-7
12. Scott SB, Sørensen JE, Rao RR, Moon C, Kibsgaard J, Shao-Horn Y, et al. The low overpotential regime of acidic water oxidation part II: trends in metal and oxygen stability numbers. Energy Environ Sci. 2022;15(5):1988-2001. https://doi.org/10.1039/d1ee03915f

13. Geiger S, Kasian O, Ledendecker M, Pizzutilo E, Mingers AM, Fu WT, et al. The stability number as a metric for electrocatalyst stability benchmarking. Nat Catal. 2018;1(7):508-15. https://doi.org/10.1038/s41929-018-0085-6
14. Escalera-López D, Czioska S, Geppert J, Boubnov A, Röse P, Saraçi E, et al. Phase- and surface composition-dependent electrochemical stability of Ir-Ru nanoparticles during oxygen evolution reaction. ACS Catal. 2021;11(15):9300-16. https://doi.org/10.1021/acscatal.1c01682
15. Liu Y, Li X, Jang H, Wu J, Kim MG, Xi X, et al. Self-limiting surface leaching stabilizes Ru-based catalysts for acidic water oxidation. Energy Environ Sci. 2025;18(7):3352-64. https://doi.org/10.1039/d4ee05220j
16. Over H. Surface chemistry of ruthenium dioxide in heterogeneous catalysis and electrocatalysis: from fundamental to applied research. Chem Rev. 2012;112(6):3356-426. https://doi.org/10.1021/cr200247n
17. Li L, Zhang G, Zhou C, Lv F, Tan Y, Han Y, et al. Lanthanide-regulating Ru-O covalency optimizes acidic oxygen evolution electrocatalysis. Nat Commun. 2024;15(1):4974. https://doi.org/10.1038/s41467-024-49281-2
18. Zhu W, Song X, Liao F, Huang H, Shao Q, Feng K, et al. Stable and oxidative charged Ru enhance the acidic oxygen evolution reaction activity in two-dimensional ruthenium-iridium oxide. Nat Commun. 2023;14(1):5365. https://doi.org/10.1038/s41467-023-41036-9
19. Rao RR, Kolb MJ, Giordano L, Pedersen AF, Katayama Y, Hwang J, et al. Operando identification of site-dependent water oxidation activity on ruthenium dioxide single-crystal surfaces. Nat Catal. 2020;3(6):516-25. https://doi.org/10.1038/s41929-020-0457-6
20. Lin Z, Chaudhary P, Vigil SA, Fratarcangeli M, Soderstedt CJ, Alexandrov V, et al. Understanding the reaction energetics of oxygen-evolving electrocatalysts. Energy Environ Sci. 2025;18(16):8029-38. https://doi.org/10.1039/d5ee02196k
21. Ping X, Liu Y, Zheng L, Song Y, Guo L, Chen S, et al. Locking the lattice oxygen in RuO2 to stabilize highly active Ru sites in acidic water oxidation. Nat Commun. 2024;15(1):2501. https://doi.org/10.1038/s41467-024-46815-6
22. Wang Y, Yang R, Ding Y, Zhang B, Li H, Bai B, et al. Unraveling oxygen vacancy site mechanism of Rh-doped RuO2 catalyst for long-lasting acidic water oxidation. Nat Commun. 2023;14(1):1412. https://doi.org/10.1038/s41467-023-37008-8
23. Yuan B, Dang Q, Liu H, Sendeku MG, Peng J, Fan Y, et al. Synergistic niobium and manganese co-doping into RuO2 nanocrystal enables PEM water splitting under high current. Nat Commun. 2025;16(1):4583. https://doi.org/10.1038/s41467-025-59710-5
24. Zheng W, Zhao Y, Jiang K, Xie F, Meng L, Gao S, et al. Heteroatom dopants overcome the activity-stability trade-off in RuO2 for acidic oxygen evolution. Nat Commun. 2025;16(1):6716. https://doi.org/10.1038/s41467-025-62036-x

25. Liu Y, Wang Y, Li H, Kim MG, Duan Z, Talat K, et al. Effectiveness of strain and dopants on breaking the activity-stability trade-off of RuO2 acidic oxygen evolution electrocatalysts. Nat Commun. 2025;16(1):1717. https://doi.org/10.1038/s41467-025-56638-8
26. Jin H, Liu X, An P, Tang C, Yu H, Zhang Q, et al. Dynamic rhenium dopant boosts ruthenium oxide for durable oxygen evolution. Nat Commun. 2023;14(1):354. https://doi.org/10.1038/s41467-023-35913-6
27. Hu W, Huang B, Sun M, Du J, Hai Y, Yin W, et al. Doping Ti into RuO2 to accelerate bridged-oxygen-assisted deprotonation for acidic oxygen evolution reaction. Adv Mater. 2025;37(3):2411709. https://doi.org/10.1002/adma.202411709
28. Shi Z, Li J, Wang Y, Liu S, Zhu J, Yang J, et al. Customized reaction route for ruthenium oxide towards stabilized water oxidation in high-performance PEM electrolyzers. Nat Commun. 2023;14(1):843. https://doi.org/10.1038/s41467-023-36380-9
29. Shen Y, Zhang XL, Qu MR, Ma J, Zhu S, Min YL, et al. Cr dopant mediates hydroxyl spillover on RuO2 for high-efficiency proton exchange membrane electrolysis. Nat Commun. 2024;15(1):7861. https://doi.org/10.1038/s41467-024-51871-z
30. Wu H, Chang J, Yu J, Wang S, Hu Z, Waterhouse GIN, et al. Atomically engineered interfaces inducing bridging oxygen-mediated deprotonation for enhanced oxygen evolution in acidic conditions. Nat Commun. 2024;15(1):10315. https://doi.org/10.1038/s41467-024-54798-7
31. Lin C, Li JL, Li X, Yang S, Luo W, Zhang Y, et al. In-situ reconstructed Ru atom array on α-MnO2 with enhanced performance for acidic water oxidation. Nat Catal. 2021;4(12):1012-23. https://doi.org/10.1038/s41929-021-00703-0
32. Hao Y, Hung SF, Wang L, Deng L, Zeng WJ, Zhang C, et al. Designing neighboring-site activation of single atom via tunnel ions for boosting acidic oxygen evolution. Nat Commun. 2024;15(1):8015. https://doi.org/10.1038/s41467-024-52410-6
33. Wang K, Wang Y, Yang B, Li Z, Qin X, Zhang Q, et al. Highly active ruthenium sites stabilized by modulating electron-feeding for sustainable acidic oxygen-evolution electrocatalysis. Energy Environ Sci. 2022;15(6):2356-65. https://doi.org/10.1039/d1ee03610f
34. Liu Z, Liu H, Zhou K, Liu M, Xue T, Zhang J, et al. Data- and theory-guided design of dual-role V-doped RuO2 for high-performance acidic oxygen evolution. Angew Chem Int Ed Engl. 2026;65(32):e8887957. https://doi.org/10.1002/anie.8887957
35. Kresse G, Furthmüller J. Efficient iterative schemes for ab initio total-energy calculations using a plane-wave basis set. Phys Rev B. 1996;54(16):11169-86. https://doi.org/10.1103/physrevb.54.11169
36. Kresse G, Hafner J. Ab initio molecular-dynamics simulation of the liquid-metal–amorphous-semiconductor transition in germanium. Phys Rev B. 1994;49(20):14251-69. https://doi.org/10.1103/physrevb.49.14251

37. Blöchl PE. Projector augmented-wave method. Phys Rev B. 1994;50(24):17953-79. https://doi.org/10.1103/physrevb.50.17953
38. Perdew JP, Burke K, Ernzerhof M. Generalized Gradient Approximation Made Simple. Phys Rev Lett. 1996;77(18):3865-8. https://doi.org/10.1103/physrevlett.77.3865
39. Zhao ZL, Wang Q, Huang X, Feng Q, Gu S, Zhang Z, et al. Boosting the oxygen evolution reaction using defect-rich ultra-thin ruthenium oxide nanosheets in acidic media. Energy Environ Sci. 2020;13(12):5143-51. https://doi.org/10.1039/d0ee01960g
40. Yang J, An K, Yu Z, Qiao L, Cao Y, Zhuang Y, et al. Effect of cation and anion vacancies in ruthenium oxide on the activity and stability of acidic oxygen evolution. ACS Catal. 2024;14(23):17739-47. https://doi.org/10.1021/acscatal.4c02779
41. Chen D, Yu R, Yu K, Lu R, Zhao H, Jiao J, et al. Bicontinuous RuO2 nanoreactors for acidic water oxidation. Nat Commun. 2024;15(1):3928. https://doi.org/10.1038/s41467-024-48372-4
42. Fairhurst AR, Snyder J, Wang C, Strmcnik D, Stamenkovic VR. Electrocatalysis: from planar surfaces to nanostructured interfaces. Chem Rev. 2025;125(3):1332-419. https://doi.org/10.1021/acs.chemrev.4c00133
43. Liu J, Wang T, Liu X, Shi H, Li S, Xie L, et al. Reducible Co3+–O sites of Co–Ni–P–Ox on CeO2 nanorods boost acidic water oxidation via interfacial charge transfer-promoted surface reconstruction. ACS Catal. 2023;13(8):5194-204. https://doi.org/10.1021/acscatal.2c06133

Supplementary Files

This is a list of supplementary files associated with this preprint. Click to download.

- RuMnVO2DiscoverElectrochemistrySI.docx